Fire Behavior of Prestressed Iron-Based Shape Memory Alloy (Fe-SMA)

Elyas GHAFOORI [1], Martin NEUENSCHWANDER [2], Moslem SHAHVERDI [1,3], Christoph CZADERSKI [1], Mario FONTANA [4]

[1] Structural Engineering Research Laboratory, Swiss Federal Laboratories for Materials Science and Technology (Empa), Duebendorf, Switzerland

[2] University of California Berkeley, Pacific Earthquake Engineering Research Center, 325 Davis Hall, Berkeley, CA 94720, United States

[3] School of Civil Engineering, University of Tehran, 16th Azar Street, Tehran, Iran

[4] ETH Zurich, Swiss Federal Institute of Technology Zurich, 8093 Zürich, Switzerland

Contact e-mail: elyas.ghafoori@empa.ch

ABSTRACT: iron-based shape memory alloy (Fe-SMA) members have been recently introduced for prestressed strengthening of civil structures such as buildings and bridges. As civil structures are often prone to elevated temperatures when exposed to fire, the high-temperature behavior of the structural elements including all the materials used for rehabilitation is of great importance. Therefore, this study provides the first systematic study on the structural fire behavior of the prestressed Fe-SMA members. A series of transient total deformation tests was conducted on Fe-SMA strips with two thicknesses of 0.5 and 1.5 mm. The Fe-SMA strips were first activated and then prestressed. The transient tests were then performed for service loads of 0, 80 and 240 N/mm2 and heating rates of 5, 15 and 50 °C/min.

Keywords: Iron-based shape memory alloy (Fe-SMA); elevated temperatures; fire; pre-stressed strengthening.

1 INTRODUCTION

Buildings and bridges often require a substantial rehabilitation at some point in their service life. This occurs for a number of reasons, including general aging, increased service load limits, corrosion of metallic components or fatigue to name but a few. In order to address this problem, municipalities often look for effective retrofit solutions rather than replacing entire structures. This is because the effort in terms of time and costs for retrofits is often by far lower than for the complete replacement of an old structure with a new one. Therefore, developing novel and innovative retrofit solutions is paramount to increase the lifetime of existing civil structures (Cladera et al., 2014).

Previous studies have shown that the application of carbon fiber-reinforced polymer (CFRP) strips considerably enhances the service and ultimate load capacity of metallic (Zhao, 2013) and concrete (Teng et al., 2003) structures. Moreover, prestressing CFRP-strips can further increase the efficiency of the CFRP-retrofit solution. It has been shown that prestressed CFRP-strips

enhance the buckling strength (Ghafoori and Motavalli, 2015a, Ghafoori and Motavalli, 2015c, Ghafoori and Motavalli, 2015b), fatigue behavior (Ghafoori et al., 2015, Hosseini et al., 2017, Ghafoori et al., 2018) and the flexural capacity (Ghafoori and Motavalli, 2013) of metallic structural members, as well as the load-bearing capacity of concrete structures in general (Gallego et al., 2016, Michels et al., 2013, Czaderski and Motavalli, 2007, Czaderski et al., 2006). Furthermore, in reinforced concrete, crack width can be closed and structural deformations can be reduced. However, oftentimes hydraulic jacks are required to prestress the CFRP strips. And in some cases, this might simply not be possible (e.g., due to lack of space) or makes the strengthening procedure overly complex. Recently, the shape memory effect (SME) of shape memory alloys (SMAs) was innovatively exploited for the first time to prestress-strengthen structural members, opening an avenue to overcome the aforementioned drawbacks related to hydraulic jacks.
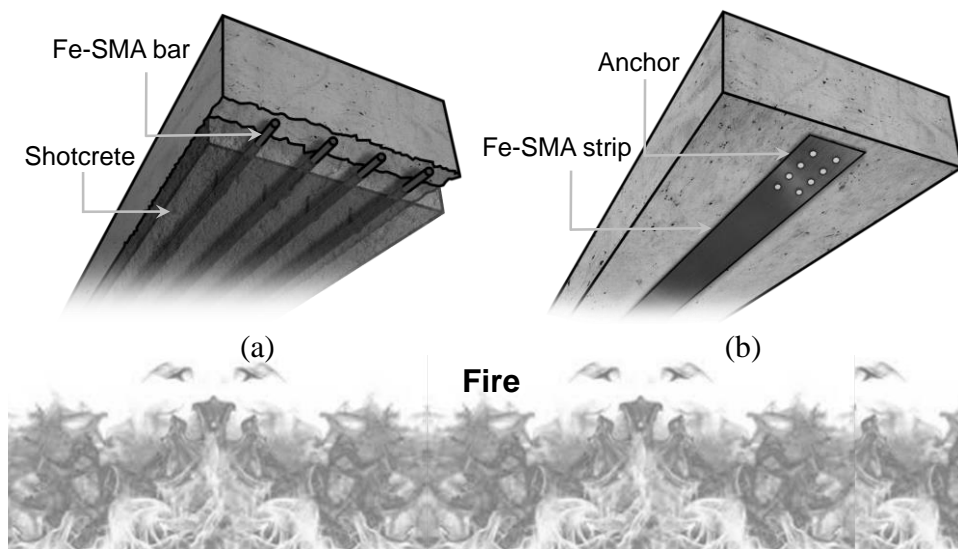
Figure 1. Scheme of concrete slabs strengthened by prestressed a) Fe-SMA rebars, and b) Fe-SMA strips exposed to fire (Ghafoori et al., 2019)

SMAs are intelligently engineered metals that can recover their initial shape (after being deformed permanently) through a thermal activation process, consisting of a heating and subsequent cooling phase (Ghafoori et al., 2017). Upon heating, the shape memory effect of an SMA (Sato et al., 1982) is triggered by the reverse transformation of a prior deformation-induced forward phase transformation from austenite to martensite at lower temperatures.

A Fe-17Mn-5Si-10Cr-4Ni-1(V,C) SMA, referred to as Fe-SMA hereafter, has been developed at Empa (Dong et al., 2009, Lee et al., 2013b, Lee et al., 2013a, Leinenbach et al., 2012), and is to date commercially available in the form of ribbed bars (Julien Michels and Raafat) and strips (re-fer AG Company). So far, it has been shown that prestressed Fe-SMA elements can be used as internal (e.g., (Shahverdi et al., 2016b, Shahverdi et al., 2016a, Czaderski et al., 2014)) and external (e.g., (Michels et al., 2018)) reinforcement of concrete structures, as well as, as external reinforcement for metallic structures (e.g., (Izadi et al., 2018c, Izadi et al., 2018b, Izadi et al., 2018a)). As illustrated in Fig. 1, Fe-SMA bars and strips can be attached, for example, to existing concrete slabs using a shotcrete layer (Shahverdi et al., 2016a, Shahverdi et al., 2016b) in case of rebars or an end anchorage system (Michels et al., 2018) in case of strips. Fe-SMA strips can be attached to existing metallic structures using different types of mechanical anchorage systems (e.g., (Izadi et al., 2018b, Izadi et al., 2018c)).

Thus far, extensive experimental studies with Fe-SMA material have been conducted, characterizing its mechanical properties at ambient temperature (Shahverdi et al., 2018), the phase transformation involved (Czaderski et al., 2014), the achievable recovery stress level (Lee et al., 2013b), its creep and relaxation (Leinenbach et al., 2016) as well as low-cycle (Hosseini et al., 2018), finite element modeling (Abouali et al., 2019) and high-cycle fatigue (Ghafoori et al., 2017) behavior. However, because civil structures are potentially subject to the fire hazard (see Fig. 1), the alloy's still unstudied basic elevated-temperature mechanical properties must be explored before it can be used in engineering practice in innovative prestressing retrofits on a regular basis. The present work provides a first contribution to fill this knowledge gap and is focused on the structural fire behavior of the aforementioned pioneering strengthening-retrofits of concrete slabs (Michels et al., 2018, Shahverdi et al., 2016a, Shahverdi et al., 2016b).

Table 1. Overview of the tested samples

Test	Parameters	Number of Specimens
Transient test	Service load: 0, 80, 240 N/mm²	2 per test
Activated material 1.5 mm thickness	Heating rate: 5, 15, 50 °C/min	Total: 18

2 TEST PROGRAM

Table 1 gives an overview of the parameters of the entire test program. This article only presents briefly the test plan and result for the Fe-SMA strip with 1.5-mm thickness; readers can refer to (Ghafoori et al., 2019) for more details related to test plan and results (including strips with 0.5-mm thickness). Transient total deformation tests are often performed to characterize the transient behavior of structural materials when subjected to a fire exposure. More information about this type of the tests (i.e., test purpose and procedure) can be found in (Ghafoori et al., 2019).

The procedure of the transient tests with activated Fe-SMA material consists of four steps which simulate, in a broader sense, the fire exposure of prestressed Fe-SMA members. This section aims at providing more specific technical information about the test procedure and parameters. The discussion will be illustrated with Fig. 2a showing a schematic view of the stress-strain behavior during the pre-straining and unloading (Step 1), the thermal activation process (Step 2), the application of the service load (Step 3) and the transient total deformation tests (Step 4), together with an indication of the mechanical properties.

In the *first step*, extending from 0-B in Fig. 2a, the material is pre-strained at room temperature with a constant strain rate of 0.5 %/min until a total strain of 2% (path 0-A) and then unloaded again using the same strain rate (path A-B).

During the pre-straining along path 0-A, a forward martensitic transformation occurs and the material is said to be in a martensite state after that. In addition to the stress-strain response of the material during pre-straining, Fig. 2.a defines the different mechanical properties that can be derived from this stage of the test. They comprise: (1) the Young's modulus, E, determined as the slope of the initial linear part of the stress-strain diagram (see Fig. 2.a); (2) the proportionality limit, f_p, defined, where the stress-strain curve first deviates from the linear elastic line of slope equal to the Young's modulus; (3) the 0.2 % yield strength, $f_{y,0.2}$, determined as the intersection of the stress-strain curve and a straight line with a slope equal to the Young's modulus and an offset on the abscissa from the origin by 0.2%; and (4) the stress in the specimen, σ_{pre}, at a total strain level of ε_{pre}=2%.

Path A-B shows the unloading process to a low stress level of σ_0=50 N/mm². The reason to not completely unload the specimen to zero stress follows from the feature of the test setup that it can only transmit tensile and no compressive forces. Therefore, a minimal tensile stress must be applied in order to prevent the specimen from becoming loose in the test apparatus during the

early stages of the subsequent thermal activation process, when yet no contraction of the SME masks the relaxing effect of the thermal expansion of the alloy. A transition phase had to be built into the test procedure at the end of the unloading process, because time-dependent contraction, ε_{shrk}, occurred. In order to prevent a force increase, the specimen was held in force-controlled mode for five minutes until the contraction had decayed (see path B-C in Fig. 2a), before the machine was switched into the displacement-controlled mode for the subsequent thermal activation process The contraction under a constant stress is related to the decay of time-dependent reverse phase transformation (Hosseini et al., 2018).
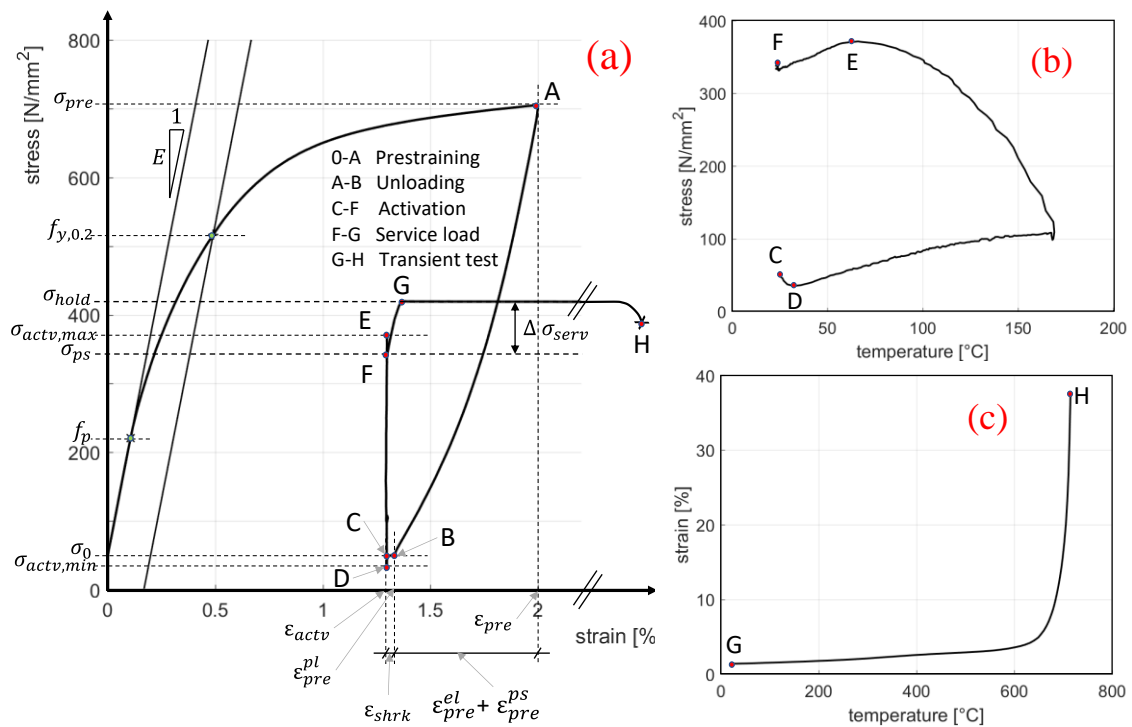
Figure 2. Test procedure of the transient tests on the activated Fe-SMA strips: a) the stress-strain behavior (during prestraining, unloading, activation process, application of the service load and the transient test) with the indication of the mechanical properties, b) the stress-temperature behavior during the activation process, and c) the strain temperature behavior during the total transient deformation test (Ghafoori et al., 2019)

In the *second step*, the specimen was heated up and cooled down, as illustrated in Fig. 2b with a representative stress–temperature curve during the activation process extending from C-F. During this entire step, the machine remained in a displacement-controlled mode and the specimen strain was held constant at ε_{actv}. During the heating phase of the activation process, the specimen was heated with a rate of 10 °C/min to the target temperature of 160 °C. Next, the furnace was opened in order to let the entire test setup cool down to ambient temperature during 2 hours. After that the furnace was closed again for a conditioning period of 30 min to let the furnace temperature stabilize completely. Figure 2b shows the evolution of the specimen stress with temperature during the entire activation process. In Fig. 2a., $\sigma_{actv,min}$, $\sigma_{actv,max}$ and σ_{ps} refer to the minimum, maximum and final stress during the activation process. Figure 2c shows the strain temperature behavior during the total transient deformation test.

In the *third step*, additional service load increments of $\Delta\sigma_{serv}$=0, 80 and 240 N/mm² were applied with a strain-rate of 0.5 %/min at room temperature, in order to simulate different service load

levels during a fire exposure. The resulting total 'hold' stress level, including recovery and service stresses, is then called σ_{hold}. Figure 2a shows an example of a test, during which a service load increment of 80 N/mm^2 was applied in the third step (path F-G).

Finally, the *fourth step*, extending along the path G-H in Figs. 2a and c, is the actual transient total deformation test, simulating the fire exposure. In this step, the machine was in a force-controlled mode, in order to keep the stress in the specimen constant, while it was heated with different constant heating rates of 5, 15 or 50 °C/min until failure. Thereby, the specimen strain was continuously recorded with the extensometer until an elongation limit of 5.5 mm, after which the extensometer was removed to prevent possible damage to the device due to abrupt specimen rupture. More details about the test setup, specimens, procedures and parameters can be found in (Ghafoori et al., 2019).

3 TEST RESULTS

The current total deformation of a carbon steel specimen, recorded during a total transient deformation test (increasing temperature under constant load), consists of the three different components of thermal strain (ε_{th}), stress-induced mechanical strain ($\varepsilon_{mech} = \varepsilon_{el} + \varepsilon_{pl}$) and creep strain ($\varepsilon_{cr}$) (Anderberg, 1988). In the case of a shape memory alloy, however, an additional strain component needs to be considered that covers the phase–change-induced transformation strain (ε_{tr}). Hence, the total deformation of the Fe-SMA can be written as:

$$\varepsilon(\sigma, \theta, t) = \varepsilon_{th}(\theta) + \varepsilon_{mech}(\sigma, \theta) + \varepsilon_{tr}(\sigma, \theta) + \varepsilon_{cr}(\sigma, \theta, t) \tag{1}$$

where θ is the temperature, σ is the stress and t is the time. Leinenbach et al. (Leinenbach et al., 2016) have shown that the main source of the time-dependent creep strain $\varepsilon_{cr}(\sigma, \theta, t)$ is transformation-induced creep (TRIC), which itself is also dependent on the temperature and the stress level applied. Regarding the phase–change-induced strain component, it has been concluded in an earlier study by some of the present authors (Lee et al., 2013a) that the transformation strain, ε_{tr}, is a function of the stress level and the maximum temperature reached during activation (Hosseini et al., 2018).

Table 2. Results of the activation and transient tests on the Fe-SMA strips with the thickness of 1.5 mm (Ghafoori et al., 2019)

σ_{serv}	[N/mm^2]	$\dot{\theta} = 5\,°C/min$			$\dot{\theta} = 15\,°C/min$			$\dot{\theta} = 50\,°C/min$			Average
		0	80	240	0	80	240	0	80	240	
f_p	[N/mm^2]	233.6	237.7	237.7	232.9	243.4	231.2	224.8	244.3	238.7	236
$f_{y,0.2}$	[N/mm^2]	515.7	522.4	511.6	515.6	527.8	508.4	513.2	515.8	510.4	515.6
E	[N/mm^2]	172,757	168,417	184,640	177,575	168,754	174,353	181,323	169,224	177,098	174,904.6
$\sigma_{actv,max}$	[N/mm^2]	386.4	382.5	386.0	391.2	394.3	393.5	393.0	380.4	387.8	388.3
σ_{ps}	[N/mm^2]	373.6	365.3	372.8	373.9	377.9	358.6	375.6	360.8	373.7	370.2
σ_{hold}	[N/mm^2]	373.6	445.3	612.8	373.9	457.9	598.6	375.6	440.8	613.6	-
$\sigma_{hold}/f_{y,0.2}$	[-]	0.72	0.85	1.20	0.72	0.87	1.18	0.73	0.86	1.20	-
θ_{creep}	[°C]	653	618	527	658	613	528	667	624	559	-
θ_{crit}	[°C]	701	668	598	714	674	601	731	691	610	-

Table 2 shows the total strain–temperature behavior of the transient total deformation tests on activated Fe-SMA strips (with σ_{ps} ranging from 358.6 to 377.9 N/mm^2) with a thickness of 1.5 mm, subjected to additional different service load levels of 0, 80, and 240 N/mm^2 and heating rates of 5, 15 and 50 °C. The onset temperature of high-temperature creep was determined using

a graphical technique and will be referred to as 'creep temperature' in this study and are shown in Table 2. The creep temperature was defined as the temperature, at which the tangent slope of a total strain–temperature curve exceeded a threshold value of 0.5×10^{-3} °C^{-1} (Zemp, 2017). With a similar graphical procedure, the failure temperatures were determined and presented in Table 2. The failure was defined when the tangent slope of total strain–temperature curve exceeded a threshold value of 0.012 °C^{-1} (Zemp, 2017).

This table indicates the minimum creep and failure temperatures for the specimens of 1.5 mm as 527 and 598 °C, respectively. Furthermore, Table 2 shows that a creep temperature higher than 500 °C was observed consistently in the tests, irrespective of the service load levels or heating rates applied. And the failure temperatures were approximately 50-80 °C higher than the corresponding creep temperatures.

Furthermore, Table 2 illustrates that both creep and failure temperatures decrease with an increase in the service load level. Furthermore, it can be concluded that different heating rates do not significantly affect creep and failure temperatures. For all of the specimens, the failure temperatures were approximately 50-70 °C higher than the corresponding creep temperatures. For more details about the test results and analysis related to prestress loss in the Fe-SMA members subjected to a fire exposure can be found in (Ghafoori et al., 2019).

4   CONCLUSIONS

In this study, a series of transient total deformation tests was conducted on the prestressed Fe-SMA strips with two thicknesses of 0.5 and 1.5 mm. The transient tests were performed for the service loads of 0, 80 and 240 N/mm^2 and heating rates of 5, 15 and 50 °C/min.

From the transient total deformation tests, the mean high-temperature creep onset-temperatures and failure temperatures of the 1.5 mm and 0.5 mm specimens were approximately 527 and 598 °C and 517 and 596 °C, respectively. For all different service load levels and heating rates examined, a high-temperature creep onset-temperature greater than 500 °C was observed, and the corresponding failure temperatures exceeded the latter by approximately 50-70 °C. It was observed that both high-temperature creep onset-temperatures and failure temperatures decreased with increasing service load levels, whereas the heating rate had no significant influence. More details about the test procedure and results can be found in (Ghafoori et al., 2019).

5   ACKNOWLEDGMENTS

6   REFERENCES

re-fer AG Company. *www.re-fer.eu/en* [Online]. [Accessed].
ABOUALI, S., SHAHVERDI, M., GHASSEMIEH, M. & MOTAVALLI, M. 2019. Nonlinear simulation of reinforced concrete beams retrofitted by near-surface mounted iron-based shape memory alloys. *Engineering Structures,* 187**,** 133-148.
ANDERBERG, Y. 1988. Modelling steel behaviour. *Fire Safety Journal,* 13**,** 17-26.
CLADERA, A., WEBER, B., LEINENBACH, C., CZADERSKI, C., SHAHVERDI, M. & MOTAVALLI, M. 2014. Iron-based shape memory alloys for civil engineering structures: An overview. *Construction and Building Materials,* 63**,** 281-293.
CZADERSKI, C., HAHNEBACH, B. & MOTAVALLI, M. 2006. RC beam with variable stiffness and strength. *Construction and Building Materials,* 20**,** 824-833.
CZADERSKI, C. & MOTAVALLI, M. 2007. 40-Year-old full-scale concrete bridge girder strengthened with prestressed CFRP plates anchored using gradient method. *Composites Part B: Engineering,* 38**,** 878-886.

CZADERSKI, C., SHAHVERDI, M., BRÖNNIMANN, R., LEINENBACH, C. & MOTAVALLI, M. 2014. Feasibility of iron-based shape memory alloy strips for prestressed strengthening of concrete structures. *Construction and Building Materials,* 56**,** 94-105.

DONG, Z., KLOTZ, U. E., LEINENBACH, C., BERGAMINI, A., CZADERSKI, C. & MOTAVALLI, M. 2009. A novel Fe-Mn-Si shape memory alloy with improved shape recovery properties by VC precipitation. *Advanced Engineering Materials,* 11**,** 40-44.

GALLEGO, J. M., CZADERSKI, C. & MICHELS, J. 2016. Prestress force-release tests at elevated temperatures - Gradient anchorage stability for prestressed EB CFRP strips. *Composite Structures,* 137**,** 159-169.

GHAFOORI, E., HOSSEINI, A., AL-MAHAIDI, R., ZHAO, X. L. & MOTAVALLI, M. 2018. Prestressed CFRP-Strengthening and Long-Term Wireless Monitoring of an Old Roadway Metallic Bridge *Engineering Structures,* accepted.

GHAFOORI, E., HOSSEINI, E., LEINENBACH, C., MICHELS, J. & MOTAVALLI, M. 2017. Fatigue behavior of a Fe-Mn-Si shape memory alloy used for prestressed strengthening. *Materials & Design,* 133**,** 349-362.

GHAFOORI, E. & MOTAVALLI, M. 2013. Flexural and interfacial behavior of metallic beams strengthened by prestressed bonded plates. *Composite Structures,* 101**,** 22-34.

GHAFOORI, E. & MOTAVALLI, M. 2015a. Innovative CFRP-Prestressing System for Strengthening Metallic Structures. *Journal of Composites for Construction,* 19**,** 04015006.

GHAFOORI, E. & MOTAVALLI, M. 2015b. Lateral-torsional buckling of steel I-beams retrofitted by bonded and un-bonded CFRP laminates with different pre-stress levels: experimental and numerical study. *Construction and Building Materials,* 76**,** 194–206.

GHAFOORI, E. & MOTAVALLI, M. 2015c. Normal, high and ultra-high modulus CFRP laminates for bonded and un-bonded strengthening of steel beams. *Materials and Design,* 67**,** 232–243.

GHAFOORI, E., MOTAVALLI, M., NUSSBAUMER, A., HERWIG, A., PRINZ, G. S. & FONTANA, M. 2015. Design criterion for fatigue strengthening of riveted beams in a 120-year-old railway metallic bridge using pre-stressed CFRP plates. *Composites Part B: Engineering,* 68**,** 1-13.

GHAFOORI, E., NEUENSCHWANDER, M., SHAHVERDI, M., CZADERSKI, C. & FONTANA, M. 2019. Elevated temperature behavior of an iron-based shape memory alloy used for prestressed strengthening of civil structures. *Construction and Building Materials,* 211**,** 437-452.

HOSSEINI, A., GHAFOORI, E., MOTAVALLI, M., NUSSBAUMER, A. & ZHAO, X.-L. 2017. Mode I fatigue crack arrest in tensile steel members using prestressed CFRP plates. *Composite Structures,* 178**,** 119-134.

HOSSEINI, E., GHAFOORI, E., LEINENBACH, C., MOTAVALLI, M. & HOLDSWORTH, S. R. 2018. Stress recovery and cyclic behaviour of an Fe–Mn–Si shape memory alloy after multiple thermal activation. *Smart Materials and Structures,* 27**,** 025009.

IZADI, M. R., GHAFOORI, E., HOSSEINI, A., MICHELS, J. & MOTAVALLI, M. 2018a. Thermally-Activated Iron-Based Shape Memory Alloy for Strengthening of Metallic Girders *Thin-Walled Structures,* Submitted for publication.

IZADI, M. R., GHAFOORI, E., MOTAVALLI, M. & MAALEK, S. 2018b. Iron-based shape memory alloy for the fatigue strengthening of cracked steel plates: Effects of re-activations and loading frequencies. *Engineering Structures,* accepted for publication. https://doi.org/10.1016/j.engstruct.2018.09.021.

IZADI, M. R., GHAFOORI, E., SHAHVERDI, M., MOTAVALLI, M. & MAALEK, S. 2018c. Development of an iron-based shape memory alloy (Fe-SMA) strengthening system for steel plates. *Engineering Structures,* 174**,** 433-446.

JULIEN MICHELS, M. S. C. C. & RAAFAT, E.-H. Mechanical Performance of Iron-Based Shape-Memory Alloy Ribbed Bars for Concrete Prestressing. *Materials Journal,* 115**,** 877-886.

LEE, W. J., WEBER, B., FELTRIN, G., CZADERSKI, C., MOTAVALLI, M. & LEINENBACH, C. 2013a. Phase transformation behavior under uniaxial deformation of an Fe–Mn–Si–Cr–Ni–VC shape memory alloy. *Materials Science and Engineering: A,* 581**,** 1-7.

LEE, W. J., WEBER, B., FELTRIN, G., CZADERSKI, C., MOTAVALLI, M. & LEINENBACH, C. 2013b. Stress recovery behaviour of an Fe–Mn–Si–Cr–Ni–VC shape memory alloy used for prestressing. *Smart Materials and Structures, IOP Science,* 22**,** 1-9.

LEINENBACH, C., KRAMER, H., BERNHARD, C. & EIFLER, D. 2012. Thermo-mechanical properties of an Fe-Mn-Si-Cr-Ni-VC shape memory alloy with low transformation temperature. *Advanced Engineering Materials,* 14**,** 62-67.

LEINENBACH, C., LEE, W. J., LIS, A., ARABI-HASHEMI, A., CAYRON, C. & WEBER, B. 2016. Creep and stress relaxation of a FeMnSi-based shape memory alloy at low temperatures. *Materials Science and Engineering A,* 677**,** 106-115.

MICHELS, J., SENA-CRUZ, J., CZADERSKI, C. & MOTAVALLI, M. 2013. Structural strengthening with prestressed CFRP strips with gradient anchorage. *Journal of Composites for Construction,* 17**,** 651-661.

MICHELS, J., SHAHVERDI, M. & CZADERSKI, C. 2018. Flexural strengthening of structural concrete with iron-based shape memory alloy strips. *Structural Concrete,* 19**,** 876-891.
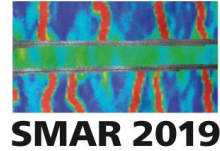
SATO, A., CHISHIMA, E., SOMA, K. & MORI, T. 1982. Shape memory effect in $\gamma \rightleftarrows \epsilon$ transformation in Fe-30Mn-1Si alloy single crystals. *Acta Metallurgica,* 30**,** 1177-1183.

SHAHVERDI, M., CZADERSKI, C., ANNEN, P. & MOTAVALLI, M. 2016a. Strengthening of RC beams by iron-based shape memory alloy bars embedded in a shotcrete layer. *Engineering Structures,* 117**,** 263-273.

SHAHVERDI, M., CZADERSKI, C. & MOTAVALLI, M. 2016b. Iron-based shape memory alloys for prestressed near-surface mounted strengthening of reinforced concrete beams. *Construction and Building Materials,* 112**,** 28-38.

SHAHVERDI, M., MICHELS, J., CZADERSKI, C. & MOTAVALLI, M. 2018. Iron-based shape memory alloy strips for strengthening RC members: Material behavior and characterization. *Construction and Building Materials,* 173**,** 586-599.

TENG, J. G., CHEN, J. F., SMITH, S. T. & LAM, L. 2003. Behaviour and strength of FRP-strengthened RC structures: a state-of-the-art review. *Proceedings of the Institution of Civil Engineers - Structures and Buildings,* 156**,** 51-62.

ZEMP, V. 2017. *Behavior of Iron-Based Shape Memory Alloy Subjected to Elevated Temperatures, Master Thesis.* Master Thesis, ETH Zurich.

ZHAO, X. L. 2013. *FRP-Strengthened Metallic Structures,* Boca Raton, FL, Taylor and Francis.